Realization and Characterization of a Bulk-Type All-Silicon High Pressure Sensor

Elena Chan, Dequan Lin, Lei Lu, *Member, IEEE*, Deqiang Zhang, Shichao Guo, Yiming Zhang, Kevin Chau, and Man Wong, *Senior Member, IEEE*

***Abstract*— Distinct from conventional diaphragm-type pressure sensors, a silicon-based bulk-type high pressure sensor has been analyzed, realized, and characterized. External hydrostatic pressure acting on the sensor is converted to a biaxial compression inside an all-silicon encapsulated vacuum cavity. The stress anisotropy is analytically modeled and numerically simulated. The biaxial compression is measured using two pairs of piezoresistors oriented to optimally utilize the anisotropy of silicon piezoresistance. An improved pressure seal in the test-package allowed extended testing of the sensor up to a pressure of 200 MPa and a temperature of 175 °C. Reported also is a zero-offset of the sensor, largely attributed to the tensile stress induced by the insulating cover oxide after cooling from the high-temperature dopant activation anneal. [2017-0253]**

***Index Terms*— Pressure sensor, piezoresistive, MEMS, silicon, bulk, eutectic bonding.**

I. Introduction

CONVENTIONAL diaphragm-type MEMS pressure sensors are not ideal for measuring pressure higher than 100 MPa, such as those encountered in heavy machineries, automobiles and oil exploration. As the pressure rating is increased, the lateral dimensions and thickness of the sensing diaphragm must be respectively reduced and increased to avoid failure. As a result, the deformation and stress largely localized on the diaphragm at lower operating pressure are increasingly extended to the bulk of the sensor. Such delocalization degrades the performance and narrows the design window of both piezoresistive and capacitive MEMS pressure sensors.

Manuscript received October 12, 2017; revised November 28, 2017; accepted December 9, 2017. Date of publication January 18, 2018; date of current version April 2, 2018. This work was supported in part by the Key Research Program of Chinese Academy of Sciences under Grant ZDRW-ZS-2016-1-3 and in part by the Strategic Priority Research Program of Chinese Academy of Sciences under Grant XDA14040200. Subject Editor P. M. Sarro.

(Corresponding authors: Elena Chan; Man Wong.)

E. Chan and M. Wong are with the Department of Electronic and Computer Engineering, The Hong Kong University of Science and Technology, Hong Kong (e-mail: ylechanaa@connect.ust.hk; eemwong@ece.ust.hk).

D. Lin is with the Key Laboratory of Petroleum Resource Research, Institute of Geology and Geophysics, Chinese Academy of Sciences, Beijing, China, and also with the University of Chinese Academy of Sciences, Beijing, China (e-mail: lindq4123@mail.iggcas.ac.cn).

L. Lu is with the Department of Electronic and Computer Engineering, The Hong Kong University of Science and Technology, Hong Kong, and also with the HKUST Jockey Club Institute for Advanced Study, Hong Kong, China.

D. Zhang is with Beijing Sllaid Science and Technology Co., Ltd., Beijing, China.

S. Guo and Y. Zhang are with the Key Laboratory of Petroleum Resource Research, Institute of Geology and Geophysics, Chinese Academy of Sciences, Beijing, China.

K. Chau is with the Key Laboratory of Petroleum Resource Research, Institute of Geology and Geophysics, Chinese Academy of Sciences, Beijing, China, and also with the Department of Electronic and Computer Engineering, The Hong Kong University of Science and Technology, Hong Kong (e-mail: zhouxl@mail.iggcas.ac.cn).

Color versions of one or more of the figures in this paper are available online at http://ieeexplore.ieee.org.

Digital Object Identifier 10.1109/JMEMS.2017.2786730

TABLE I
Comparison of MEMS Piezoresistive High-Pressure Sensors

Ref.	Type	P_{max} (MPa)	V_{out} (mV)	Power Supply	T (°C)
[2]	Si-Glass Diaphragm	150	50	5 V	20~150
[3]	Si-Glass Diaphragm	150	167	1.5 mA	≤ 200
[4]	Si-Glass Bulk	200	22	5 V	N/A
[5]	Si-Glass Bulk	60	62	5 V	−40~125
[1]	All-Si Bulk	120	58	5 V	25~125
This Work	All-Si Bulk	200	79	5 V	25~175

A comparison of the characteristics of representative MEMS high-pressure sensors is listed in Table I. They are all based on the piezoresistive principle. An all-silicon (Si) bulk-type sensor [1] that does not require fragile deformable diaphragm-like micro-structures is more suitable for measuring pressure beyond 100 MPa. Overload protection is a natural advantage of this type of sensors, providing higher operational tolerance and robustness. In diaphragm-type sensors [2], [3], the Si diaphragm thickness of 200 to 350 μm is significant in comparison with the die thickness. To strengthen the support rim surrounding the thick diaphragm, the Si die is bonded to a glass substrate. The bulk-type sensors in [4] and [5] also involve a bonded Si-on-glass die stack. Since the Young's moduli of Si and glass are different, the stress associated with the bending deformation of the composite structure induced by hydrostatic pressure is sensed using piezoresistors constructed on the Si side of the sensor die. In all cases, sensors that involve bonding of Si and glass are burdened by the inherent difference between the coefficients of thermal expansion of dissimilar materials.

In place of a construction involving bonding of heterogeneous materials, the theoretical feasibility of a variety of

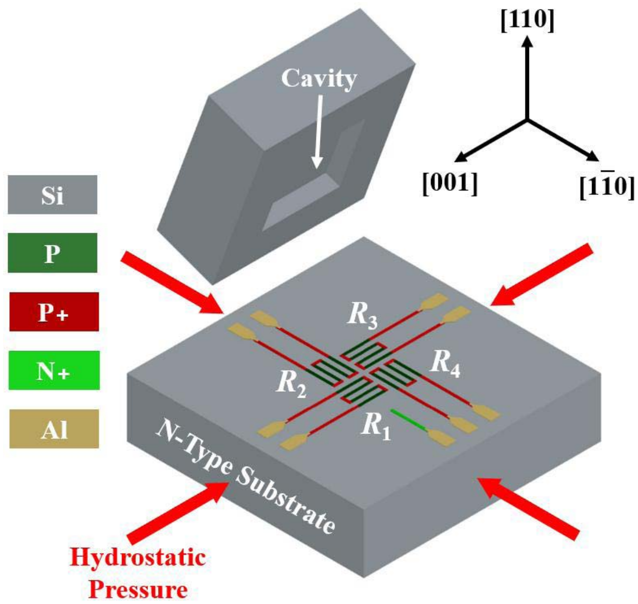

Fig. 1. Schematic pressure sensor die with the cap detached and the cover oxide removed for visualization of the piezoresistors.

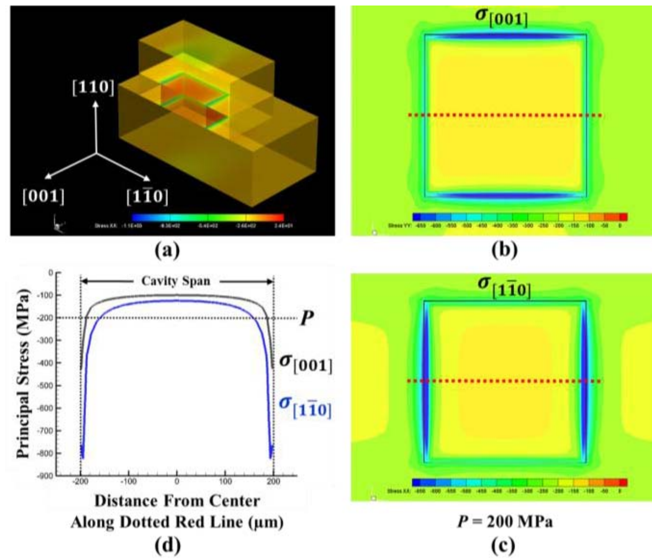

Fig. 2. Distribution of FEA-simulated principal stress components on the surface of the [110]-oriented device die inside a 400-μm $\times$ 400-μm cavity subjected to $P = 200$ MPa. The height of the cavity is 200 μm. (a) FEA model. (b)-(c) 2-dimensional distribution of $\sigma_{[001]}$ and $\sigma_{[1\bar{1}0]}$, respectively, inside the cavity. (d) $\sigma_{[001]}$ and $\sigma_{[1\bar{1}0]}$ plotted along the respective dotted lines.

bulk-type all-Si pressure sensor constructions has been discussed [6], and the first demonstration and characterization of such a sensor has recently been reported [1]. However, the capability of the sensor was not fully realized, due to a pressure seal failure in the test-package when exposed to a pressure load beyond 120 MPa. With an improved package construction, the functionality of the sensor is demonstrably extended up to a pressure of 200 MPa and a temperature of 175 °C. Largely attributed to the tensile stress induced by a 200-nm thick insulating cover oxide after cooling from a 1000 °C dopant activation anneal, a zero-offset is also observed in the sensor output.

II. Principle of Operation

The sensor (Fig. 1) consists of a Si "cap" eutectically vacuum-bonded [7] to a [110]-oriented Si "device" die. A deep cavity is defined in the cap, with the edges of the cavity aligned to either the Si [001] or the $\left[1\bar{1}0\right]$ crystal orientation. Junction-isolated piezoresistors, R_1 and R_3 aligned to the former and R_2 and R_4 aligned to the latter, are realized on the top surface of the device die exposed inside the cavity. Upon the application of a hydrostatic pressure (P) on the sensor, an internal stress field (σ) is generated that would have been a uniform triaxial compression equal to P in the absence of the cavity. The vacuum-sealed cavity zeroes out those components of σ associated with the [110] surface-normal orientation on the device die, thus resulting in a biaxial stress field with $\sigma_{[1\bar{1}0]}$ and $\sigma_{[001]}$ as the two principal components.

Since all the other stress components are zero except $\sigma_{[1\bar{1}0]}$ and $\sigma_{[001]}$, the corresponding strain components $\varepsilon_{[1\bar{1}0]}$ and $\varepsilon_{[001]}$ are given by

$$\begin{pmatrix} \varepsilon_{[1\bar{1}0]} \\ \varepsilon_{[001]} \end{pmatrix} = \begin{pmatrix} s_{11} & s_{12} \\ s_{12} & s_{22} \end{pmatrix} \begin{pmatrix} \sigma_{[1\bar{1}0]} \\ \sigma_{[001]} \end{pmatrix}, \tag{1}$$

where the values of s_{11}, s_{12} and s_{22} in the compliance matrix of the [110]-oriented Si are taken to be $5.891\times$, $-2.142\times$ and 7.642×10^{-12} Pa^{-1} respectively.

Since $s_{11} \neq s_{22}$, the biaxial stress field resulting from P is anisotropic, even at the center of the exposed surface of the device die. The surface deformation along the two orthogonal orientations is, however, coupled and constrained, such that $\varepsilon_{[1\bar{1}0]} \approx \varepsilon_{[001]}$ for a cavity with a square base. Consequently, the anisotropy of the biaxial stress can be estimated using (1):

$$\frac{\sigma_{[1\bar{1}0]}}{\sigma_{[001]}} \approx \frac{s_{22} - s_{12}}{s_{11} - s_{12}} = 1.22. \tag{2}$$

I.e., $\sigma_{[1\bar{1}0]}$ is $\sim 22\%$ larger in magnitude than $\sigma_{[001]}$.

Finite-element analysis (FEA) was used to simulate the distributions of $\sigma_{[1\bar{1}0]}$ and $\sigma_{[001]}$ (Fig. 2) inside a cavity with a 400-μm $\times$ 400-μm square base and a 200-μm height. Since a Wheatstone bridge is used to connect the two pairs of piezoresistors shown in Fig. 1, the fact that $\sigma_{[1\bar{1}0]}$ and $\sigma_{[001]}$ are relatively flat around the center of the cavity is desirable for the construction of a "balanced" bridge, the output of which is relatively insensitive to lithographic misalignment in the placement of the resistors.

When subjected to $P = 200$ MPa, $\sigma_{[1\bar{1}0]}$ and $\sigma_{[001]}$ at the center of the cavity are -126 and -100 MPa, respectively. The simulated magnitude of the former is $\sim$26% larger than that of the latter, close to the $\sim$22% estimated analytically. It is clear that the magnitude of both is smaller than P. This is because the "bulging" of the exposed surface of the device die towards the interior of the cavity caused by the zeroing of the normal stress component results in the superposition of a tensile stress that partially compensates, hence reduces, the biaxial compression. At the expense of a higher device complexity, a double-cavity design [6] could be implemented to alleviate this compensation effect.

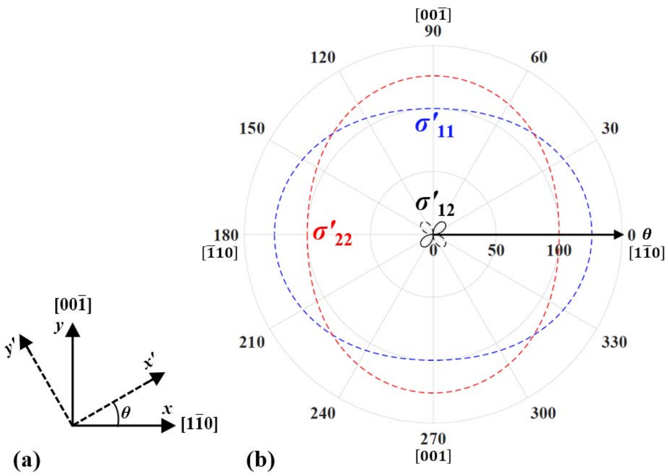

Fig. 3. (a) Rotation of a resistor by an angle θ on the [110]-oriented device die. (b) Polar plots of the stress components in MPa, with dashed line indicating negative values.

The stress field acting on a piezoresistor placed at an arbitrary angle θ (Fig. 3a) w.r.t. the [1$\bar{1}$0] principal axis is given by

$$\begin{pmatrix}\sigma'_{11}\\ \sigma'_{22}\\ \sigma'_{12}\end{pmatrix} = \begin{pmatrix}\cos^2\theta & \sin^2\theta & \sin 2\theta\\ \sin^2\theta & \cos^2\theta & -\sin 2\theta\\ -(\sin 2\theta)/2 & (\sin 2\theta)/2 & \cos 2\theta\end{pmatrix}\begin{pmatrix}\sigma_{[1\bar{1}0]}\\ \sigma_{[001]}\\ 0\end{pmatrix}, \tag{3}$$

where σ'_{11}, σ'_{22} and σ'_{12}, the respective longitudinal, transverse and shear stress components, are plotted in Fig. 3b using the simulated values of $\sigma_{[1\bar{1}0]} = -126$ MPa and $\sigma_{[001]} = -100$ MPa at $\theta = 0°$.

When subjected to a generalized stress field $\sigma = (\sigma_{11}, \sigma_{22}, \sigma_{33}, \sigma_{23}, \sigma_{13}, \sigma_{12})^T$, a piezoresistor exhibits a change, $\Delta\rho = (\Delta\rho_{11}, \Delta\rho_{22}, \Delta\rho_{33}, \Delta\rho_{23}, \Delta\rho_{13}, \Delta\rho_{12})^T$, in its resistivity ($\rho$). The relative change in resistivity $\Delta\rho/\rho$ and σ are related by $\Delta\rho/\rho = \pi\sigma$, where π is the 6×6 piezoresistive coefficient matrix. Again using primed variables when referring to a θ-oriented piezoresistor, the $\Delta\rho'/\rho$ in the longitudinal direction (length-wise along the resistor) is given by

$$\frac{\Delta\rho'_{11}}{\rho} = \pi'_{11}\sigma'_{11} + \pi'_{12}\sigma'_{22} + \underbrace{\pi'_{13}\sigma'_{33} + \pi'_{14}\sigma'_{23} + \pi'_{15}\sigma'_{13}}_{=0} + \pi'_{16}\sigma'_{12}, \tag{4}$$

where it is noted that in the present design, the stress components $(\sigma'_{33}, \sigma'_{23}, \sigma'_{13})$ associated with the normal [110]-orientation are zero. The respective longitudinal, transverse and shear piezoresistive coefficients π'_{11}, π'_{12} and π'_{16} are given by

$$\pi'_{11} = \pi_{11} - \frac{1}{2}(\pi_{11} - \pi_{12} - \pi_{44})\cos^2\theta\left(3\sin^2\theta + 1\right), \tag{5}$$

$$\pi'_{12} = \pi_{12} + \frac{3}{8}(\pi_{11} - \pi_{12} - \pi_{44})\sin^2 2\theta, \tag{6}$$

$$\pi'_{16} = \frac{1}{4}(\pi_{11} - \pi_{12} - \pi_{44})\sin 2\theta\,(1 - 3\cos 2\theta), \tag{7}$$

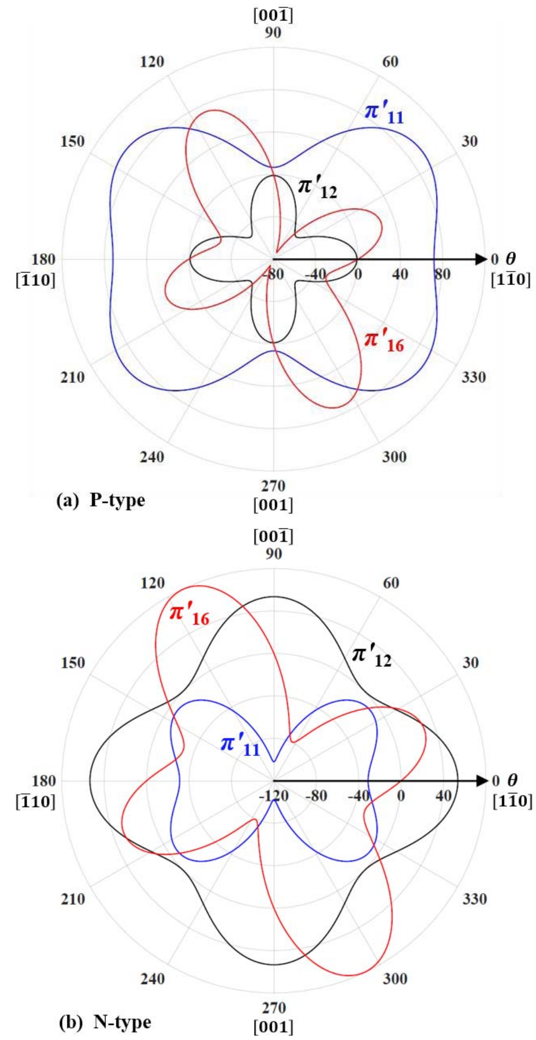

Fig. 4. Polar plots of π'_{11}, π'_{12} and π'_{16} on (a) p-type and (b) n-type (110) silicon surface in 10^{-11} Pa^{-1}.

TABLE II

π_{11}, π_{12} AND π_{44} OF SINGLE-CRYSTALLINE SILICON AT ROOM TEMPERATURE [8]

Piezoresistive coefficients (10^{-11} Pa^{-1})	P-silicon 7.8 Ω·cm	N-silicon 11.7 Ω·cm
π_{11}	6.6	–102.2
π_{12}	–1.1	53.4
π_{44}	138.1	–13.6
$\pi_{11} - \pi_{12} - \pi_{44}$	–130.4	–142.0

where the values of the fundamental piezoresistive coefficients π_{11}, π_{12} and π_{44} for single-crystalline silicon are listed in Table II, and the corresponding polar plots for π'_{11}, π'_{12} and π'_{16} are shown in Fig. 4.

Combining σ' in Fig. 3 and π' in Fig. 4, the percentage change $\Delta\rho'_{11}/\rho$ on the device die for P= 200 MPa is obtained and plotted in Fig. 5.

For both p- and n-type piezoresistors, the largest difference in $\Delta\rho'_{11}/\rho$ is obtained between those oriented along the

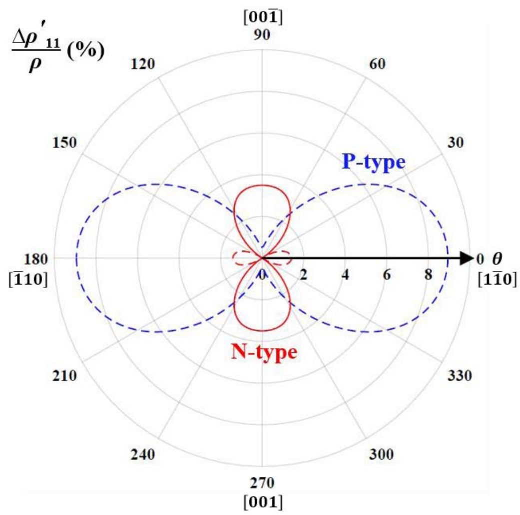

Fig. 5. Polar plots of the longitudinal $\Delta\rho'_{11}/\rho$ for p- and n-type piezoresistors on the [110]-oriented device die subjected to $P = 200$ MPa, with the solid and dashed lines indicating respective positive and negative values.

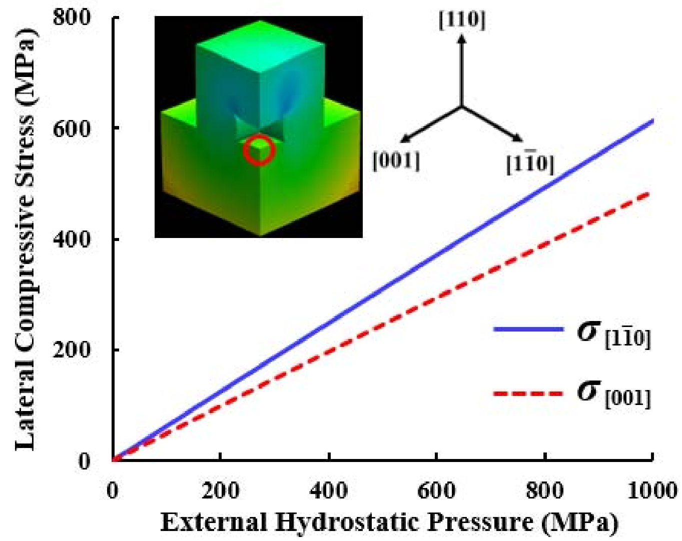

Fig. 6. FEA-simulated principal stress components at the center of the cavity on the [110]-oriented device die versus P up to 1 GPa. The values are taken from inside the red circle indicated in the quarter-model of the sensor.

[1$\bar{1}$0] and [001] directions, hence the preferred orthogonal piezoresistor orientation in the present design. The output voltage (V_{OUT}) of the Wheatstone bridge is proportional to the absolute magnitude of this difference, which is ~8.4% for p-type but only ~4.9% for n-type piezoresistors. The raw sensitivity with p-type piezoresistors is therefore ~1.7 times larger than that with n-type piezoresistors. This difference can be mostly attributed to $\sigma_{[1\bar{1}0]}$ being ~26% larger in magnitude than $\sigma_{[001]}$ in the present design. The raw sensitivities with p- and n-type piezoresistors would otherwise be comparable had $\sigma_{[1\bar{1}0]}$ and $\sigma_{[001]}$ been equal. Consequently, p-type piezoresistors are selected in the present implementation. Furthermore, it is apparent from Fig. 5 that the p-type piezoresistors along the [001] orientation are almost unchanged over P. This is not the case for the n-type piezoresistors.

The ultimate strength of the sensor subjected to hydrostatic pressure loading was also studied using FEA. The results are shown in Fig. 6.

The cap and device die are both 500-μm thick, and the respective cavity length, width and height are 400, 400 and 200 μm. The magnitudes of both $\sigma_{[1\bar{1}0]}$ and $\sigma_{[001]}$ at the center of the device die continue to increase linearly with P, while the stress remains compressive throughout the body of the sensor. In particular, the maximum downward deformation at the top of the cavity is only ~1.6 μm at $P = 1$ GPa. Therefore, it can be concluded that the sensor can potentially withstand P of at least 1 GPa.

III. Device Fabrication

The evolution of the sensor cross-section during fabrication is schematically shown in Fig. 7. Device fabrication started with a phosphorus-doped n-type [110]-oriented Si device wafer. The p-type piezoresistors and the p$^+$ diffused electrical leads were formed by boron implantation, at an energy of 40 keV and respective dose of 2.6×10^{15} and 2×10^{16} cm^{-2}. A heavily phosphorus implanted n$^+$ region was also formed to assist fixing of the electrical potential of the substrate (Fig. 7a). Two pairs of piezoresistors were fabricated, with one oriented along the [1$\bar{1}$0] orientation and the other along the orthogonal [001]. The implanted impurities were activated at 1000 °C for 30 min after the low-pressure chemical vapor deposition of a 200-nm thick silicon dioxide insulation layer. At this temperature, any residual stress in the oxide insulator was largely relaxed due to viscous flow. Contact holes were subsequently opened (Fig. 7b) before the sputtering and patterning of a 1.5-μm aluminum-silicon (Al-Si) alloy (Fig. 7c) to form both the metal pads for external electrical access and the bond ring for the aluminum-germanium (Al-Ge) eutectic bonding to the cap wafer.

Masked by patterned 3-μm thick low-temperature deposited oxide (Fig. 7d), deep reactive-ion etching was used to form the 200-μm deep cavity on a separate Si cap wafer. A layer of 500-nm Ge was subsequently evaporated (Fig. 7e), before the device and cap wafers were aligned and bonded in vacuum (Fig. 7f). Eutectic bonding was accomplished under a pressure load of 0.4 MPa at 430 °C for 5 min. Shown in Fig. 8 is a photo-micrograph of a singulated die with a superimposed layout highlighting the piezoresistors in one of the designs. The sensor measures 1.7 mm on a side.

IV. Test System and Sensor Package

Shown in Fig. 9 is a pressure sensor die mounted on and wire-bonded to a custom-made printed-circuit board (PCB). The die-attach material loses its adhesive property when soaked in acetone after wire bonding, thus resulting in a sensor die that is held only by the bond wires and effectively "suspended" in the oil medium enclosed inside a stainless steel housing. Since the die can deform freely under the applied hydrostatic pressure, the sensor is largely immune to package-induced stress, which is a major contributor to temperature-induced drifts and non-repeatability in commercial MEMS pressure sensors [9], [10].

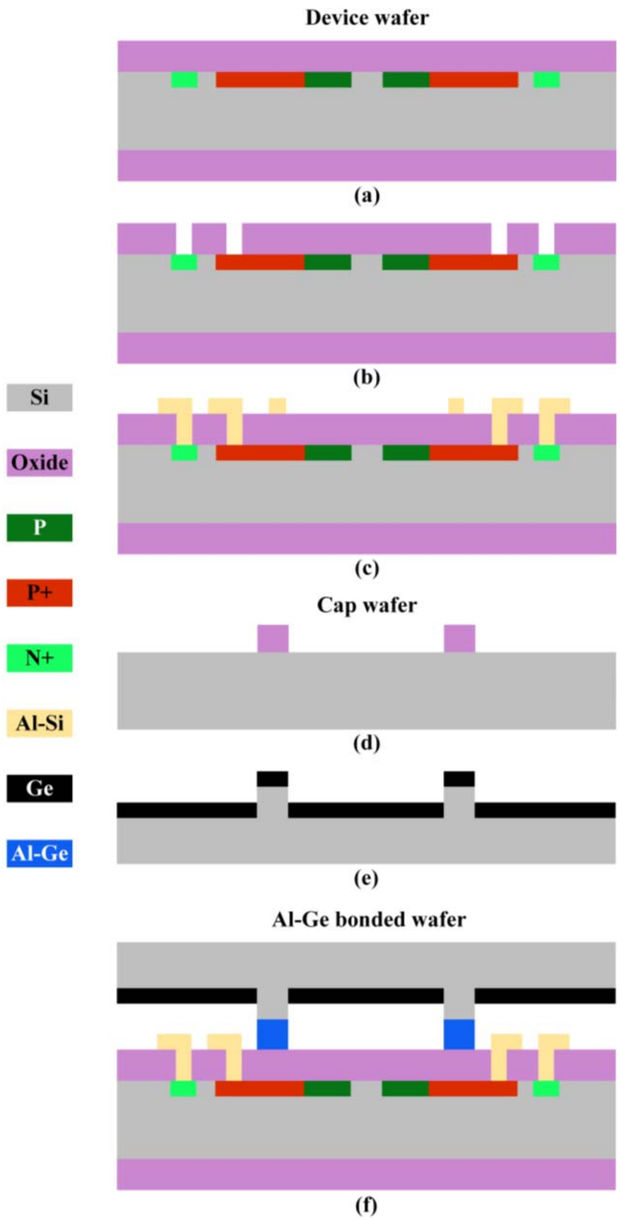

Fig. 7. Schematic cross-sections of (a)-(c) the device wafer, (d)-(e) the cap wafer, and (f) the final bonded pair.

The PCB is soldered to a high-pressure high-temperature (HPHT) connector fitted with a rubber O-ring seal for insertion into a stainless steel housing. The pressure rating of the HPHT connector was only 140 MPa, above which the O-ring seal could fail. In the present improved implementation, a much higher pressure rating of 200 MPa is achieved by forming an additional compression seal between the copper ring on the HPHT connector and the top ring inside the stainless steel housing, thus reinforcing the overall pressure seal.

A two-stage pressure generator (Fig. 10) was employed, capable of supplying pressure up to 250 MPa and consisting of a low-pressure pneumatic servo stage followed by a fixed-gain hydraulic pressure amplifier. The assembled stainless steel housing along with the packaged sensor is placed and

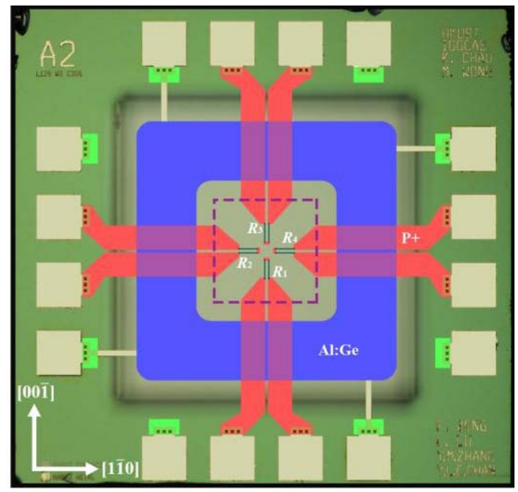

Fig. 8. Photo-micrograph of the pressure sensor die with a superimposed layout highlighting the piezoresistors. The outline of the cavity is indicated by the dotted line. The sensor measures 1.7 mm on a side.

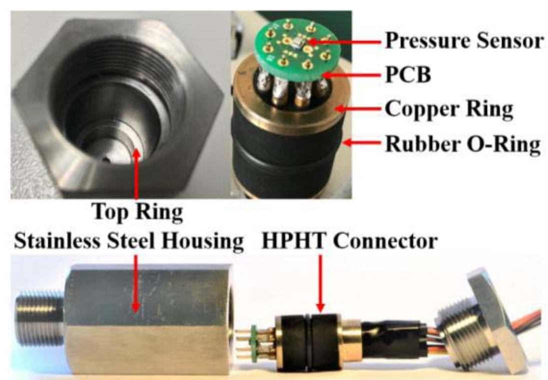

Fig. 9. Photographs of the sensor die mounted on a PCB and HPHT connector in a stainless steel housing.

connected to the outlet of the pressure generator inside a temperature chamber during testing. Silicone oil was used as the medium for transmitting the pressure to the sensor.

V. Test Results

The sensor was characterized from 0 to 200 MPa ($\sim$ 2000 atmospheres) in a temperature range of 25 to 175 °C. The measured pressure-dependence of the resistance of the piezoresistors aligned along the two principal orientations is shown in Fig. 11. Consistent with the theoretical result shown in Fig. 5, the [1$\bar{1}$0]-oriented resistors R_2 and R_4 are sensitive to the applied hydrostatic pressure, with the resistance decreasing linearly with increasing pressure, while that of the [001]-oriented resistors R_1 and R_3 remain essentially unchanged. At room temperature, the net resistance change in both R_2 and R_4 is $\sim$3.8% over the 200 MPa hydrostatic pressure. This is slightly less than half of the $\sim$8.4% estimated and shown in Fig. 5. This is reasonable, given that the piezoresistive coefficients of a highly doped piezoresistor are roughly half of those of a lightly doped one [11]. Moreover, the p$^+$ electrical leads add about 10% to the total resistance, as shown in the

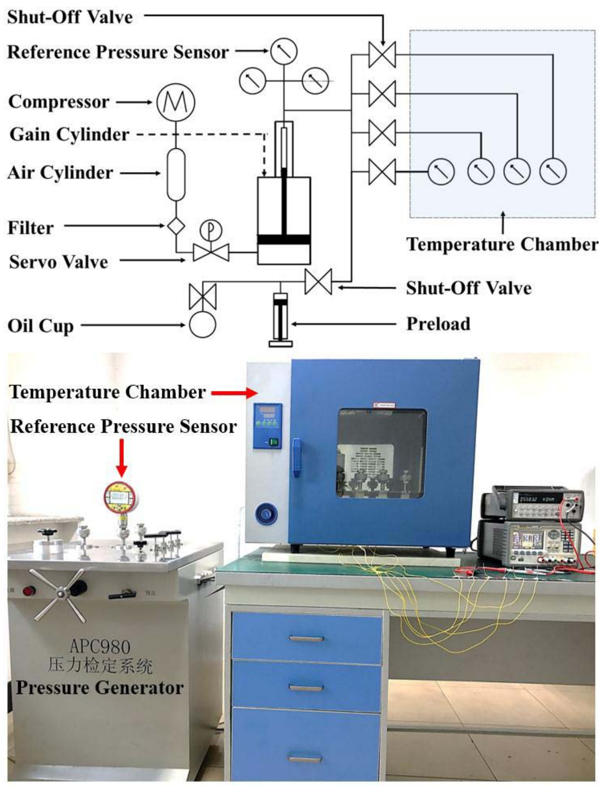

Fig. 10. A schematic diagram and a photograph of the high pressure generator and temperature chamber setup.

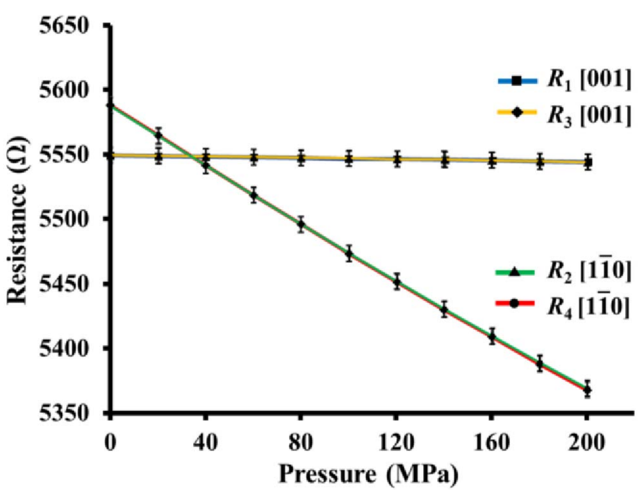

Fig. 11. Measured dependence of the resistance of R_1, R_2, R_3 and R_4 on pressure at room temperature.

layout of the piezoresistors in Fig. 8, but contribute negligibly to the resistance change over pressure.

Though the resistors are designed to have roughly the same resistance, a larger value is measured for the [1$\bar{1}$0]-oriented resistors even at $P = 0$ MPa. The resulting imbalance in the Wheatstone bridge leads to a zero-offset in V_{OUT} as shown in the histogram in Fig. 12. This offset can be largely attributed to the tensile residual stress induced by the 200-nm thick insulating cover oxide after cooling to room temperature from the 1000 °C dopant activation anneal. Only the [1$\bar{1}$0]-oriented

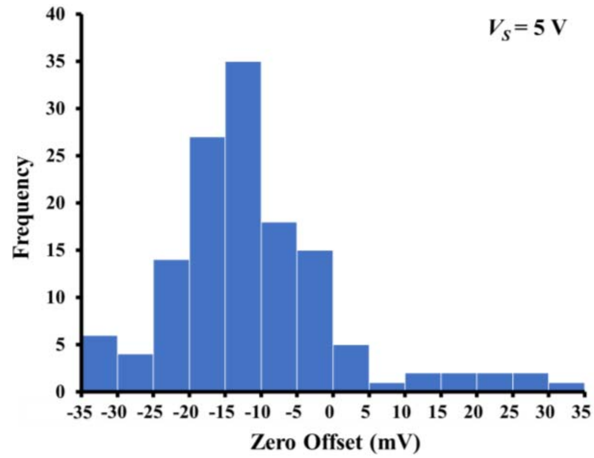

Fig. 12. Histogram of the measured zero-offset in V_{OUT} of the Wheatstone bridge at $P = 0$ MPa and room temperature for a total of 134 sensors.

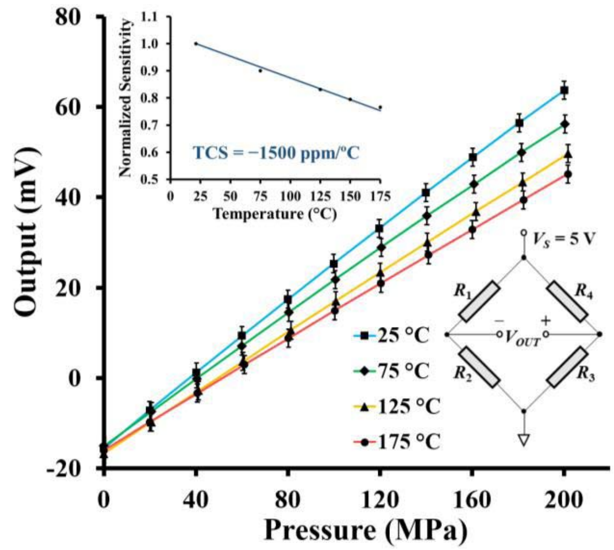

Fig. 13. Measured V_{OUT} of the pressure sensor over temperature and pressure. Shown in insets are the Wheatstone bridge configuration and the change in the pressure sensitivity over temperature.

resistors are sensitive to this residual stress. Using the FEA-estimated ratio of $\left|\sigma_{[1\bar{1}0]}\right|:P = 126:200$, the effect of this tensile residual stress, disappearing at $P \approx 35$ MPa for the resistors shown in Fig. 11, can be estimated to be equivalent to ∼22 MPa at room temperature.

The measured dependence of V_{OUT} of the Wheatstone bridge on P and temperature is plotted in Fig. 13. The corresponding slopes are extracted, yielding a sensitivity of 79 μV/V/MPa at room temperature and a temperature coefficient of sensitivity (TCS) of −1500 ppm/°C over the temperature range of 25 to 175 °C.

Consistent with the doping concentration of the piezoresistors, the measured temperature coefficients of resistance (TCR) are 1600 and 1100 ppm/°C (Fig. 14), respectively for the p$^+$ portion and the p portion of the piezoresistors. These combine to give a measured TCR of 1200 ppm/°C over the temperature range of 25 to 175 °C for the overall piezoresistor.

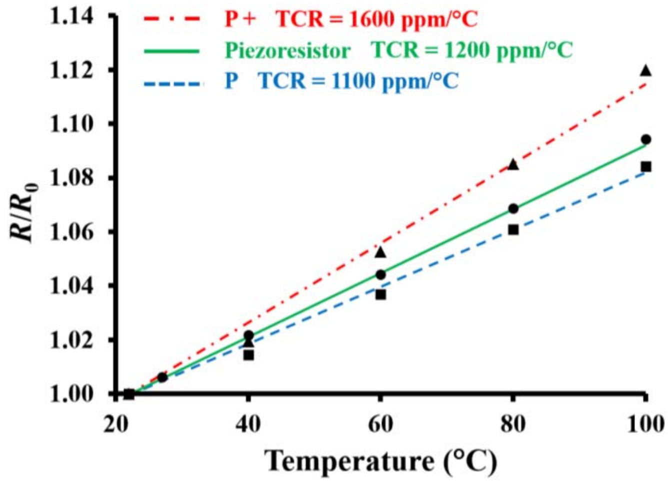

Fig. 14. Measured temperature coefficients of resistance of the p$^+$ portion, the p portion, and the overall piezoresistor.

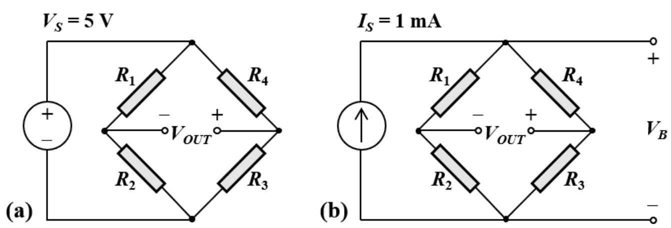

Fig. 15. Wheatstone bridge powered by (a) constant voltage source and (b) constant current source. V_B is the bridge voltage.

While the Wheatstone bridge is presently powered using a constant voltage source (Fig. 15a), it is preferably powered using a constant current source in an actual product implementation (Fig. 15b). In the latter configuration, the negative TCS (-1500 ppm/°C) can be largely offset by the positive TCR (1200 ppm/°C), thus greatly reducing to -300 ppm/°C the overall scale factor error over temperature. Furthermore, the bridge voltage V_B, providing a sensitive measure of the temperature of the piezoresistors, could be utilized for further temperature compensation, e.g., by digital means [12].

VI. Discussion and Conclusion

A bulk-type, high pressure sensor employing a single-cavity, all-silicon construction with no movable micro-structures was analyzed, realized and characterized. External hydrostatic pressure acting on the sensor is converted to a biaxial compression. The anisotropy of silicon piezoresistance was also exploited to maximize the differential output of a Wheatstone bridge formed using two pairs of orthogonally oriented piezoresistors.

A tensile residual stress is induced on the piezoresistors by the insulating cover oxide after cooling from the high-temperature dopant activation anneal. Estimated to be equivalent to $\sim$22 MPa at room temperature, this results in a $\sim$0.7% increase in the resistance of a piezoresistor aligned along the $[1\bar{1}0]$ direction. The resulting imbalance in the Wheatstone bridge leads to a systematic zero-offset in the output which does not seem to adversely affect the temperature coefficients of the pressure sensor. This offset, which is relatively small, can therefore be easily compensated in an actual product design.

The high pressure sensor, with a sensitivity of $\sim$7.9 mV/V/100 MPa, has been demonstrated to work at hydrostatic pressure loading up to 200 MPa and temperature up to 175 °C. The bulk-type, all-silicon structure has been simulated to withstand hydrostatic pressure up to 1 GPa. Hence the sensor is expected to exhibit high robustness and reliability against pressure overload.

Acknowledgment

Device fabrication was carried out at the Nanosystem Fabrication Facility (NFF) of The Hong Kong University of Science and Technology.

References

[1] D. Lin *et al.*, "A 1200-atmosphere bulk-type all-silicon pressure sensor," in *Proc. TRANSDUCERS*, Kaohsiung, Taiwan, Jun. 2017, pp. 2119–2122.

[2] T. Toriyama, K. Sawa, Y. Tanimoto, and S. Sugiyama, "A new piezoresistive high pressure sensor utilizing combination of three-axis normal stress components," in *Proc. Int. Symp. Micromechatronics Human Sci.*, Nagoya, Japan, Nov. 1999, pp. 215–220.

[3] Z. Niu, Y. Zhao, and B. Tian, "Design optimization of high pressure and high temperature piezoresistive pressure sensor for high sensitivity," *Rev. Sci. Instrum.*, vol. 85, no. 1, p. 015001, 2014.

[4] P. Heinickel and R. Werthschützky, "Functionality of a novel overload resistant silicon high pressure sensing element," in *Proc. TRANSDUCERS*, Denver, CO, USA, Jun. 2009, pp. 252–255.

[5] M. Baumann, P. Ruther, and O. Paul, "Modeling and characterization of a CMOS sensor with surface trenches for high-pressure applications," in *Proc. MEMS*, Cancun, Mexico, Jan. 2011, pp. 601–604.

[6] F. Zeng, L. Lu, Y. Zhang, S. Guo, M. Wong, and K. Chau, "MEMS pressure sensors for high-temperature high-pressure downhole applications," in *Proc. EDSSC*, Hong Kong, Aug. 2016, pp. 39–43.

[7] S. Sood, S. Farrens, R. Pinker, J. Xie, and W. Catabay, "Al-Ge eutectic wafer bonding and bond characterization for CMOS compatible wafer packaging," *ECS Trans.*, vol. 33, no. 4, pp. 93–101, 2010.

[8] C. S. Smith, "Piezoresistance effect in germanium and silicon," *Phys. Rev.*, vol. 94, no. 1, pp. 42–49, Apr. 1954.

[9] J. B. N. Ther, A. Larsen, B. Liverød, and P. Ohlckers, "Measurement of package-induced stress and thermal zero shift in transfer molded silicon piezoresistive pressure sensors," *J. Micromech. Microeng.*, vol. 8, no. 2, pp. 168–171, 1998.

[10] C. B. O'Neal, A. P. Malshe, S. B. Singh, W. D. Brown, and W. P. Eaton, "Challenges in the packaging of MEMS," in *Proc. Int. Symp. Adv. Packag. Mater.*, Braselton, GA, USA, Mar. 1999, pp. 41–47.

[11] A. A. Barlian, W.-T. Park, J. R. Mallon, Jr., A. J. Rastegar, and B. L. Pruitt, "Review: Semiconductor piezoresistance for microsystems," *Proc. IEEE*, vol. 97, no. 3, pp. 513–552, Mar. 2009.

[12] A. J. Rastegar and J. Bryzek, "A high-performance CMOS processor for piezoresistive sensors," *Sensors Mag.*, vol. 14, no. 10, pp. 82–87, Oct. 1997.

Elena Chan received the B.S. degree (Hons.) in green energy science from Hong Kong Baptist University, Hong Kong, in 2016. She is currently pursuing the M.Phil. degree with the Department of Electronic and Computer Engineering, The Hong Kong University of Science and Technology, Hong Kong. Her research interests are micro-electro-mechanical systems pressure sensor and micro-fabrication.

Dequan Lin received the B.S. degree in measurement and control technology and instrumentations from Beijing Information Science and Technology University, Beijing, China, in 2013. He is currently pursuing the M.S. degree with the University of Chinese Academy of Sciences, Beijing, and also with the Key Laboratory of Petroleum Resource Research, Institute of Geology and Geophysics, Chinese Academy of Sciences, Beijing. His research interest is MEMS pressure sensor.

Lei Lu (M'16) received the B.S. and M.S. degrees in microelectronics from Soochow University, Suzhou, China, in 2007 and 2010, respectively, and the Ph.D. degree in electronic and computer engineering (ECE) from The Hong Kong University of Science and Technology (HKUST), Hong Kong, China, in 2014.

He was an appointed Research Associate with the Department of ECE, HKUST, in 2014, and then joined the HKUST Jockey Club Institute for Advanced Study (IAS) as a Post-Doctoral Fellow in 2016. He is currently a Research Assistant Professor with the Department of ECE and concurrently appointed an IAS Junior Fellow with HKUST. His research interests include metal-oxide semiconductor materials, novel thin-film transistors, advanced displays, and MEMS sensors.

Deqiang Zhang received the B.S. degree in mechanical design from Jiamusi University, Jiamusi, China, in 2003. He was with Beijing Spake Technology Co., Ltd., Beijing, China, from 2003 to 2007. He is currently with Beijing Sllaid Science and Technology Co., Ltd., Beijing, where he develops high-precision pressure test instruments.

Shichao Guo was born in Hebei, China. He received the B.S. degree in electrical engineering from Anhui University, Hefei, China, and the M.S. degree in electrical engineering from Peking University, Beijing, China, in 2010 and 2013, respectively.

He joined the Key Laboratory of Petroleum Resource Research, Institute of Geology and Geophysics, Chinese Academy of Sciences, Beijing, in 2013, where he is involved in accelerometers and pressure sensors.

Yiming Zhang received the B.S. and Ph.D. degrees in electrical engineering from Peking University, Beijing, China, in 2007 and 2013, respectively.

In 2013, he joined the Key Laboratory of Petroleum Resource Research, Institute of Geology and Geophysics, Chinese Academy of Sciences, Beijing, China, where he is involved in accelerometers and pressure sensors.

Kevin Chau was born in Hong Kong, China. He received the B.S. degree (First Class Hons.) from the University of Hong Kong, Hong Kong, in 1980, the M.S. and Ph.D. degrees from the University of Michigan, Ann Arbor, MI, USA, in 1981 and 1987, respectively, all in electrical engineering, and the M.A. degree in music, science, and technology from Stanford University, Stanford, CA, USA, in 2013.

From 1987 to 1992, he was with the Foxboro Company, Foxboro, MA, USA, where he developed MEMS pressure sensors. From 1992 to 2006, he was with Analog Devices, Inc., MA, where he developed MEMS accelerometers, including the ADXL50, the world's first integrated surface-micromachined accelerometer. He is currently a Professor with the Key Laboratory of Petroleum Resource Research, Institute of Geology and Geophysics, Chinese Academy of Sciences, Beijing, China, and an Adjunct Professor with the Department of Electronic and Computer Engineering, The Hong Kong University of Science and Technology, Hong Kong, with research interests in MEMS and microsystems.

Dr. Chau was elected State Specially Recruited Expert under China's Thousand Talents Plan in 2014.

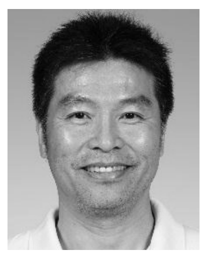

Man Wong (S'83–M'88–SM'00) was born in Beijing, China. He received the B.S. and M.S. degrees in electrical engineering from the Massachusetts Institute of Technology, Cambridge, MA, USA, from 1979 to 1984, and the Ph.D. degree in electrical engineering from the Center for Integrated Systems, Stanford University, Stanford, CA, USA, from 1985 to 1988, where he was involved in tungsten-gate MOS technology.

From 1988 to 1992, he was with the Semiconductor Process and Design Center of Texas Instruments, USA, where he was involved in the modeling and development of integrated-circuit metallization systems and dry/vapor surface-conditioning processes. He is currently with the Department of Electronic and Computer Engineering, The Hong Kong University of Science and Technology, Hong Kong. His research interests include micro-fabrication technology, device structure and material, physics and technology of thin-film transistor, organic light-emitting diode display technology, modeling and implementation of integrated micro-systems, and thin-film solar cell device and process technology. He is a member of the Tau Beta Pi, Eta Kappa Nu, and Sigma Xi.

He was appointed as an Honorary Guest Professor with Nankai University, Tianjin, China, in 2003, a Visiting Professor with Soochow University, Suzhou, China, in 2011, a Distinguished Visiting Professor with the State Key Laboratory of Transducers Technology, Institute of Microsystems and Information Technology, Chinese Academy of Sciences, Shanghai, China, in 2015, and a Visiting Professor with Xiangtang University, Xiangtang, China, in 2015.